© 2020. Published by The Company of Biologists Ltd | Journal of Experimental Biology (2020) 223, jeb215020. doi:10.1242/jeb.215020

RESEARCH ARTICLE

The sarcomere force–length relationship in an intact muscle–tendon unit

Eng Kuan Moo, Timothy R. Leonard and Walter Herzog*

ABSTRACT

The periodic striation pattern in skeletal muscle reflects the length of the basic contractile unit: the sarcomere. More than half a century ago, Gordon, Huxley and Julian provided strong support for the 'sliding filament' theory through experiments with single muscle fibres. The sarcomere force–length (FL) relationship has since been extrapolated to whole muscles in an attempt to unravel *in vivo* muscle function. However, these extrapolations were frequently associated with non-trivial assumptions, such as muscle length changes corresponding linearly to SL changes. Here, we determined the *in situ* sarcomere FL relationship in a whole muscle preparation by simultaneously measuring muscle force and individual SLs in an intact muscle–tendon unit (MTU) using state-of-the-art multi-photon excitation microscopy. We found that despite great SL non-uniformity, the mean value of SLs measured from a minute volume of the mid-belly, equivalent to about 5×10^{-6}% of the total muscle volume, agrees well with the theoretically predicted FL relationship, but only if the precise contractile filament lengths are known, and if passive forces from parallel elastic components and activation-associated sarcomere shortening are considered properly. As SLs are not uniformly distributed across the whole muscle and changes in SL with muscle length are location dependent, our results may not be valid for the proximal or distal parts of the muscle. The approach described here, and our findings, may encourage future studies to determine the role of SL non-uniformity in influencing sarcomere FL properties in different muscles and for different locations within single muscles.

KEY WORDS: Second harmonic generation imaging, Cross-bridge theory, Sliding filament theory, Muscle contraction, *In situ*, Multi-photon microscopy, Sarcomere length non-uniformity, Sarcomere length instability, Skeletal muscle properties

INTRODUCTION

The maximal active isometric force a muscle can exert depends on its length. This so-called force–length (FL) relationship is arguably the most basic mechanical property of skeletal muscles, and it has been explained with the standard 'sliding filament' theory (Gordon et al., 1966). In this theory, the amount of overlap between the contractile filaments, actin and myosin, determines uniquely the active maximal isometric force capability of a sarcomere. The sliding filament theory was formulated at the sarcomere level, but translating it to a single fibre or the whole muscle is a complex process. For example, going from the single fibre to the entire muscle level, structural and mechanical complexities are added (Blemker et al., 2005; Heemskerk et al., 2005; Lovering et al., 2013). The most important of these is that the line of action of force production in a muscle is typically not along the fibre direction as pressure, shear forces and extracellular matrix stiffness contribute to whole-muscle forces in a way not possible in a single fibre (Azizi et al., 2008; Gillies and Lieber, 2011; Holt et al., 2016; Maas et al., 2001; Purslow, 2008; Raiteri et al., 2018).

At present, our understanding of the FL relationship at the whole-muscle level has been derived primarily from experiments in which muscle forces were measured at varying muscle lengths, without direct measurement of *in situ* sarcomere length (SL) (Gokhin et al., 2009; Rack and Westbury, 1969; Sandercock and Heckman, 2001; Vaz et al., 2012; Willems and Huijing, 1994; Winters et al., 2011). In order to scale from single sarcomeres to whole muscle, researchers often relied on data from cadaveric studies in which average SL was measured in a small region of passive muscles at a given muscle length (Cutts, 1988; Lutz and Rome, 1994; Mai and Lieber, 1990; Moo et al., 2017b; Rack and Westbury, 1969; Vaz et al., 2012). These single-point data were then used to predict the mean SL for other muscle length/joint configurations, often through non-trivial assumptions: for example that SL changes linearly with the corresponding muscle length changes and that SL is independent of force. However, it has been demonstrated that the relationship between muscle length, fascicle length and the corresponding SL changes is not linear (Lichtwark et al., 2018; Moo et al., 2016; Vaz et al., 2012), and that fascicle length, and thus the mean SL in a muscle, depends crucially on muscle force (Arampatzis et al., 2006; de Brito Fontana and Herzog, 2016; Fukunaga et al., 1997). Previous attempts at relating the theoretical FL property based on average SL measurements in passive muscle to the FL properties of entire muscles has provided conflicting results, which either confirm (Winters et al., 2011) or deviate from (Rack and Westbury, 1969; Vaz et al., 2012) the theoretical predictions.

Using the sliding filament theory, whole-muscle function has been described as an up-scaled version of a single sarcomere. Gordon et al. (1966) derived the sarcomere sliding filament theory using a fibre preparation in which they argued that sarcomeres in the centre of the fibre were kept uniform and isometric using a feedback (spot follower) system to control the length of some mid-portions of the fibre. However, SL distributions are known to be non-uniform at all hierarchical levels, from myofibrils (Johnston et al., 2016; Johnston et al., 2019; Joumaa et al., 2008; Pavlov et al., 2009), to muscle fibres (Huxley and Peachey, 1961; Infantolino et al., 2010; Julian and Morgan, 1979) to whole muscles (Cromie et al., 2013; Lichtwark et al., 2018; Llewellyn et al., 2008; Moo et al., 2016). Why SL is non-uniform and what consequences this may have for the functional properties of muscles has been puzzling the muscle mechanics community for a long time, with no convincing explanation. In view of the structural and mechanical complexities, and the well-documented SL non-uniformity within myofibrils, fibres and whole

Human Performance Laboratory, Faculty of Kinesiology, University of Calgary, Calgary, AB, Canada T2N 1N4.

*Author for correspondence (wherzog@ucalgary.ca)

E.K.M., 0000-0001-6363-6063; W.H., 0000-0002-5341-0033

Received 19 September 2019; Accepted 18 February 2020

Journal of Experimental Biology (2020) 223, jeb215020. doi:10.1242/jeb.215020

muscles, studying the dynamics of sarcomeres in whole muscles and associating it with functional properties of muscles, such as the isometric FL relationship, may provide crucial insights into the 'role' of SL non-uniformity and its origins.

We recently developed imaging techniques based on multi-photon excitation microscopy that allows for the investigation of sarcomere contraction dynamics in actively contracting muscle (Moo and Herzog, 2018; Moo et al., 2017a). In the present study, we built on this imaging technique in an attempt to compare the sarcomere FL relationship of an intact muscle–tendon unit (MTU) with the theoretically predicted sarcomere FL relationship using the mean SL obtained from a small portion of the mid-belly of the contracting muscle. Based on similar studies at the single-fibre level where the plateau regions of the FL relationship are vastly extended and forces on the descending limb are much greater than theoretically predicted (Granzier and Pollack, 1990; Iwazumi and Pollack, 1981; Pollack, 1990; Ramsey and Street, 1940; ter Keurs et al., 1978), we hypothesized that the mean SL in a whole muscle was a bad predictor of the muscle's FL properties. Our experiments were done in the mouse tibialis anterior (TA) muscle using a custom-built miniature dynamometer. The mouse TA contains about 6–19 billion sarcomeres (Burkholder et al., 1994; Dumonceaux et al., 2010; Heemskerk et al., 2005; Lovering et al., 2013; Zhang et al., 2008), and we determined the individual SLs from approximately 5×10^{-6}% of those sarcomeres.

MATERIALS AND METHODS

Animal preparation

All aspects of animal care and experimental procedures were carried out in accordance with the guidelines of the Canadian Council on Animal Care and were approved by the University of Calgary's Life Sciences Animal Research and Ethics Committee. Six, 10–12 week old male C57/BL6 mice (30.5±2.6 g, mean±1 s.d.) were used. Animals were anaesthetized using a 1–2% isoflurane/oxygen mixture throughout the experiment and killed at the end of the experiment. The core temperature of the mice was maintained at about 30°C. The fascial plane between the left gluteus maximus and the anterior head of the left biceps femoris was opened for implantation of a cuff-type bipolar electrode (Herzog et al., 1992b) of 0.8 mm diameter on the sciatic nerve. The left proximal femur was fixed using a custom-made clamp at a knee flexion angle of approximately 60 deg (full knee extension: 0 deg). The left foot was pinned to a stainless steel base. The TA muscle was surgically isolated at its distal insertion with the distal tendon attached to a remnant piece of the first metatarsal bone for firm attachment to a tendon clamp extending from a 3-axis linear micro-manipulator (Newport Corp., Irvine, CA, USA). The micro-manipulator was instrumented with a uniaxial force transducer (LCFL-1kg, Omega Engineering Inc., Norwalk, CT, USA) that allowed measurement of muscle force, and a rotary stepper motor (PG25L-D24-HHC1, NMB Technologies Corporation, Novi, MI, USA) that enabled stretching of the TA at constant speed. The TA was carefully dissected from the tibia and surrounding muscles, but the proximal origin at the knee was left intact. The longitudinal axis of the TA was carefully aligned to be coaxial with the force transducer. A piece of Parafilm (VWR, Mississauga, ON, Canada) was stitched to the skin overlying the TA and attached to the tendon clamp to form a pool to accommodate a phosphate-buffered saline solution that kept the muscle hydrated and allowed for imaging using a water-immersion objective.

Imaging of *in situ* sarcomeres and force measurement at varying MTU lengths

Sarcomere images were captured and muscle forces were measured in relaxed and activated muscles at five MTU lengths. For each test, the TA was first held at a resting reference length (11–12.5 mm) before being stretched by 0.5, 1.5, 2.0, 3.0 or 4.0 mm (L1–5 groups), which corresponds to 4–36% strain, at a speed of 0.5 mm s^{-1}. When the target MTU length was reached, the TA was maximally activated using a 600 ms, continuous, supra-maximal electrical stimulation (3 times the α-motor neuron threshold, 70–80 Hz, 0.1 ms square wave pulse; Grass S88, Astro-Med. Inc., West Warwick, RI, USA) of the sciatic nerve, and sarcomere imaging was performed simultaneously. In the relaxed muscle, sarcomere imaging was performed without activation. Following sarcomere imaging and force measurement, the TA was returned to its resting reference length and a 2 min rest period was given between trials. The experimental protocol was automated by a micro-controller (TMCM-1110 stepRocker, Trinamic, Hamburg, Germany) and synchronized using an input/output interface unit (FV30-Analog, Olympus, Tokyo, Japan). Muscle forces were recorded by a data acquisition unit (DI-149, DATAQ Instruments, Inc., Akron, OH, USA) at 500 Hz throughout all trials.

During activation, muscle fibres moved proximally. In order to track the same muscle volume in the relaxed and activated muscle over multiple MTU lengths, a fluorescent marker was attached to the mid-region of the muscle using a 100 µm diameter glass pipette tip. The muscle was lit by fluorescent light (450–490 nm), and the location of the fluorescent marker was identified for the relaxed and activated muscles, thereby identifying the focal planes for subsequent sarcomere imaging. The microscope objective was then positioned at the imaging locations pre-determined by the fluorescent marker for the unstimulated and stimulated muscles in order to acquire sarcomere images at different muscle states.

Sarcomeres were visualized by second harmonic generation (SHG) imaging of the TA using an upright, multi-photon excitation microscope (FVMPE-RS model, Olympus) equipped with a wavelength-tuneable (680–1300 nm), ultrashort-pulsed (pulse width: <120 fs; repetition rate: 80 MHz) laser (InSight DeepSee-OL, Spectra-Physics, Santa Clara, CA, USA) and a 25×/1.05 NA water immersion objective (model XLPLN25XWMP2-Ultra, Olympus). The laser wavelength was 800 nm. The resulting SHG signal emitted by the muscle was collected in the backward (epi-) direction using a band-pass filter at the harmonic frequency (FF01 400/40, Semrock Inc., Rochester, NY, USA). The average laser power in the sample plane was adjusted between 15 and 18 mW to ensure optimal imaging without thermal damage to the muscle. Time-series, two-dimensional image bands were acquired in the horizontal plane (imaging area: 159 µm×2.8 µm; pixel size: 0.2 µm; bit-depth: 12; dwell time: 2 µs) at a frame rate of 23 frames s^{-1}. Images were taken from an imaging area of 159 µm×159 µm from the top 50 µm of the TA.

Analysis of muscle forces and sarcomere images

The experimental trials were divided into 10 groups based on the muscle states (relaxed versus activated) and MTU lengths (L1–5). As it is technically difficult to get good sarcomere images, we performed as many trials as possible at every MTU length. Four to six trials with good sarcomere images (i.e. good signal-to-noise ratio and minimal motion artifact) and clean muscle forces were selected for final analysis.

Derivation of active force in maximally activated MTU using two Hill-type models

Two variants of the three-element Hill-type model (standard and structural; Fig. 1A) (Winters, 1990) were used to determine the forces contributed by the passive (parallel elastic components) and contractile (sarcomere) components to the total force measured in

Journal of Experimental Biology (2020) 223, jeb215020. doi:10.1242/jeb.215020

maximally activated muscles. The standard Hill model (Fig. 1A, left) has been used by the majority of researchers while the structural Hill model (Fig. 1A, right) was thought to better represent the structural arrangement of a MTU (MacIntosh and MacNaughton, 2005; Rode et al., 2009). In the standard Hill model, the passive force is obtained from the measured maximal passive force prior to muscle activation and is termed 'standard' passive force. In contrast, the passive force of the structural Hill model takes into account the activation-induced shortening of the parallel elastic components in fixed-end contractions, and is regarded as the 'structural' passive force. The structural passive force is derived from the passive FL curve, which was approximated by a best-fitting exponential curve to the passive force–SL data, using the mean SLs measured in the activated muscle (Fig. 1B). The active force, which is defined as the force produced by the contractile components, was calculated by subtracting either the standard or the structural passive force from the total measured force.

The force–time history of each trial was divided into segments of equal interval that correspond to the acquisition time of individual sarcomere image bands (43 ms; Fig. 2). The average force within each segment was calculated and linked temporally to the morphometric measures derived from the sarcomere image that was captured within the same time interval. The 'standard' and 'structural' active forces were plotted against the mean SLs measured in the relaxed and activated muscles, respectively, and the resulting sarcomere FL curves were compared with the theoretical FL curve that was built based on thick (1.6 µm) and thin (0.95–1.2 µm) filament lengths found in the literature (Gokhin et al., 2014, 2015; Witt et al., 2006).

Morphometric measures of *in situ* sarcomeres

Planar image bands of 2.8 µm width that contained 5–30 sarcomeres in series were selected. Considering that the diameter of a myofibril is ∼1.3 µm (Powers et al., 2016), each image band was estimated to contain approximately two parallel-running myofibrils, and therefore between 10 and 60 sarcomeres. As it took approximately 200 ms for the TA to arrive at a steady state for the maximal isometric forces, sarcomeres were only visible in the activated muscles between 200 and 600 ms of the contraction (Fig. 2).

The selected image bands were band-pass-filtered using Fiji software (National Institutes of Health, Bethesda, MD, USA), and were processed using a custom-written MATLAB code (available

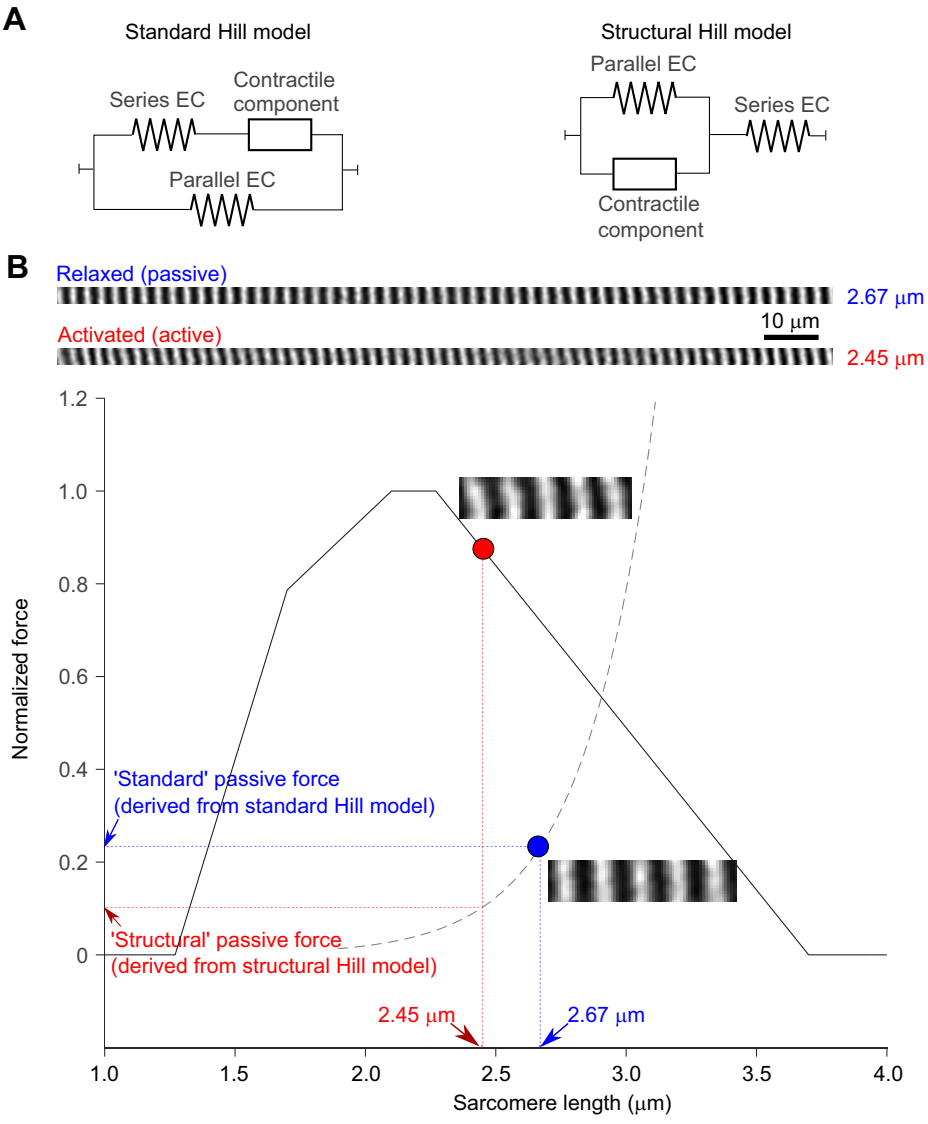

Fig. 1. Derivation of force using Hill-type models. (A) Two commonly used Hill models: standard (left) versus structural (right). In both Hill models, the active muscle force is calculated by subtracting the model-based passive force (i.e. force produced by the parallel elastic component) from the total force measured in the activated muscle. EC, elastic component. (B) Top: an example of sarcomere striation pattern captured by second harmonic generation (SHG) imaging in a relaxed and an activated muscle. As *in situ* sarcomeres shortened from a mean length of 2.67 µm to 2.45 µm during the fixed-end isometric contraction of the tibialis anterior (TA) muscle–tendon unit (MTU), the passive force derived from the structural Hill model (red, referred to as the 'structural' passive force) is lower than the passive force derived from the standard Hill model (blue, referred to as the 'standard' passive force). Because of the exponential increase in passive stiffness of the muscle, the difference between the standard and the structural passive force becomes bigger for sarcomere shortening with muscle activation at long compared with short sarcomere lengths (SLs; >2.5 µm). Note that the solid curve is the theoretical active force–length (FL) curve while the dashed line represents the exponential curve best-fitted to the passive sarcomere FL data of an individual muscle.

Journal of Experimental Biology (2020) 223, jeb215020. doi:10.1242/jeb.215020

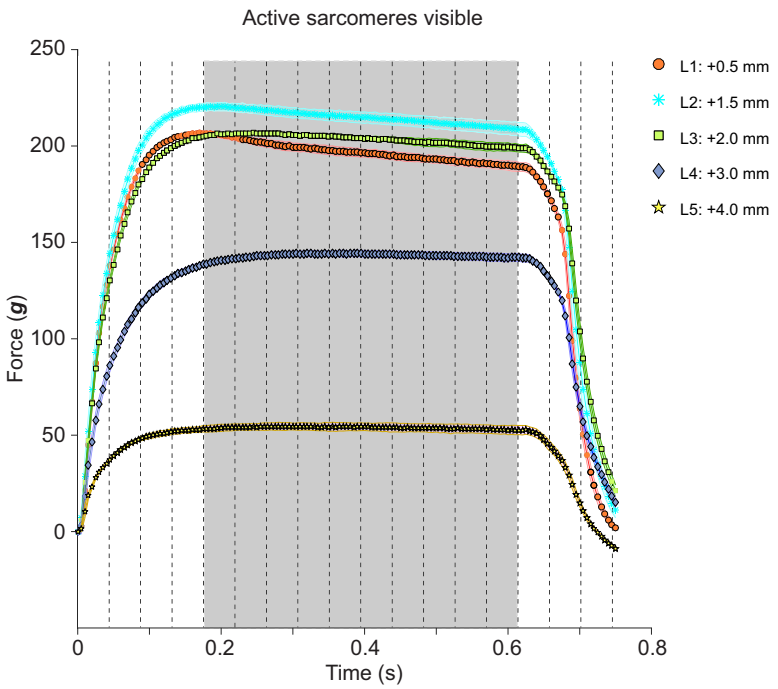

Fig. 2. Mean (±1 s.d.) 'standard' active force (shaded area) of one of the six tested muscles measured at five MTU lengths. L1–5 indicate stretch from the reference MTU length by the indicated amount. Once the muscle was electrically activated (t=0), sarcomere image bands were taken every 43 ms (marked by the evenly spaced, vertical dotted lines), and the average forces in these intervals were associated with the morphometric measures derived from the corresponding sarcomere image bands. The muscles were stimulated for approximately 600 ms but *in situ* sarcomeres were only visible when the 'standard' isometric forces reached a (near) steady state, which occurred ∼180 ms after the onset of muscle activation (grey area). Note that the standard passive forces have been subtracted from the total forces to produce the standard active forces.

from the corresponding author on request) that identified the centroids of the sarcomeric A-bands. Individual SLs were measured as the distance between adjacent A-band centroids (Cromie et al., 2013; Moo et al., 2016). As the mouse TA has a spindle-like shape (tapering from a broad, flat origin to a narrow and rounded distal tendon insertion), the surface tilt of the local muscle region was measured using a through-thickness muscle image, and SLs were corrected for out-of-plane orientation (see Fig. S1 for details).

The morphometric measures that were derived from individual sarcomere bands include the mean, s.d. and coefficient of variation (CV=s.d./mean) of SLs. Details of the number of analysed images and sarcomeres are summarized in Table 1. We report the average values of the aforementioned morphometric parameters derived from all analysed image bands. We also tested the reliability of SLs measured from SHG microscopy by imaging sarcomeres in chemically fixed fascicles using SHG and bright-field microscopy, and found that the differences of the SLs measured by the two imaging modalities were random and always less than 3% (see Table S1).

Statistical analysis

Statistical analyses were performed using SPSS (version 25, SPSS Inc., Chicago, IL, USA; SPSS code available from the corresponding author on request). Unless otherwise stated, the results were expressed as estimated marginal means (EMM)±1 standard error (s.e.). The mean values of the mean, standard deviation and CV of SLs, as well as the muscle forces were analysed for condition effects, which include muscle state (relaxed versus activated) and MTU length (L1–5), using a generalized estimating equation (GEE, under Genlin Mixed procedures in SPSS) to take into account the correlated (measurements within individual animals) nature of the observations and the unbalanced (unequal number of serial sarcomere measurements for each animal) design of the study. The mean response of the data was fitted to a linear regression model using GEE in SPSS in order to obtain the EMM and the unbiased estimates of the standard error of the variables of interest. All statistical tests were performed for two-sided testing with a type I error, α, set at 0.05 level. Multiple comparisons were accounted for through sequential Šidák adjusted P-values. As long as the data were interval type, no assumptions regarding normal distribution were needed for the GEE statistical method.

Table 1. Summary of the number of analysed images and sarcomeres in each muscle–tendon unit length group

		No. of analysed images		No. of analysed sarcomeres	
Group	Stretch (mm)	Relaxed	Activated	Relaxed	Activated
L1	0.5	602	219	1904	1534
L2	1.5	560	258	1812	2048
L3	2.0	568	264	1658	2042
L4	3.0	549	300	1658	2036
L5	4.0	545	323	1482	1960

RESULTS

Consistent with the literature, we found that the production of muscle force upon activation was dependent on muscle length (Fig. 2). SL changes were not the same as MTU length changes (Moo et al., 2016). Compared with sarcomeres in the L1 group, L5 group sarcomeres experienced strains of 43% and 51% in the relaxed and activated conditions, respectively (Fig. 3A). These values were higher than the corresponding strain applied to the MTU (36%, L5 group). The substantial shortening of SLs upon muscle activation and force production (Fig. 3A) was also MTU length dependent. During activation, sarcomeres shortened by 5–8% in the L1–4 conditions (Fig. 3A), but did not change length on average when the MTUs were stretched by 30–36% strain (L5 condition). We also measured great SL non-uniformity in our small target muscle volumes (Fig. 3B), as previously described in myofibrillar (Johnston et al., 2016; Johnston et al., 2019; Leonard and Herzog, 2010; Telley et al., 2006) and whole-muscle preparations (Lichtwark et al., 2018; Llewellyn et al., 2008; Moo and Herzog, 2018; Moo et al., 2017a).

The passive and active forces during muscle contractions were derived from the total force using the standard and the structural

Journal of Experimental Biology (2020) 223, jeb215020. doi:10.1242/jeb.215020

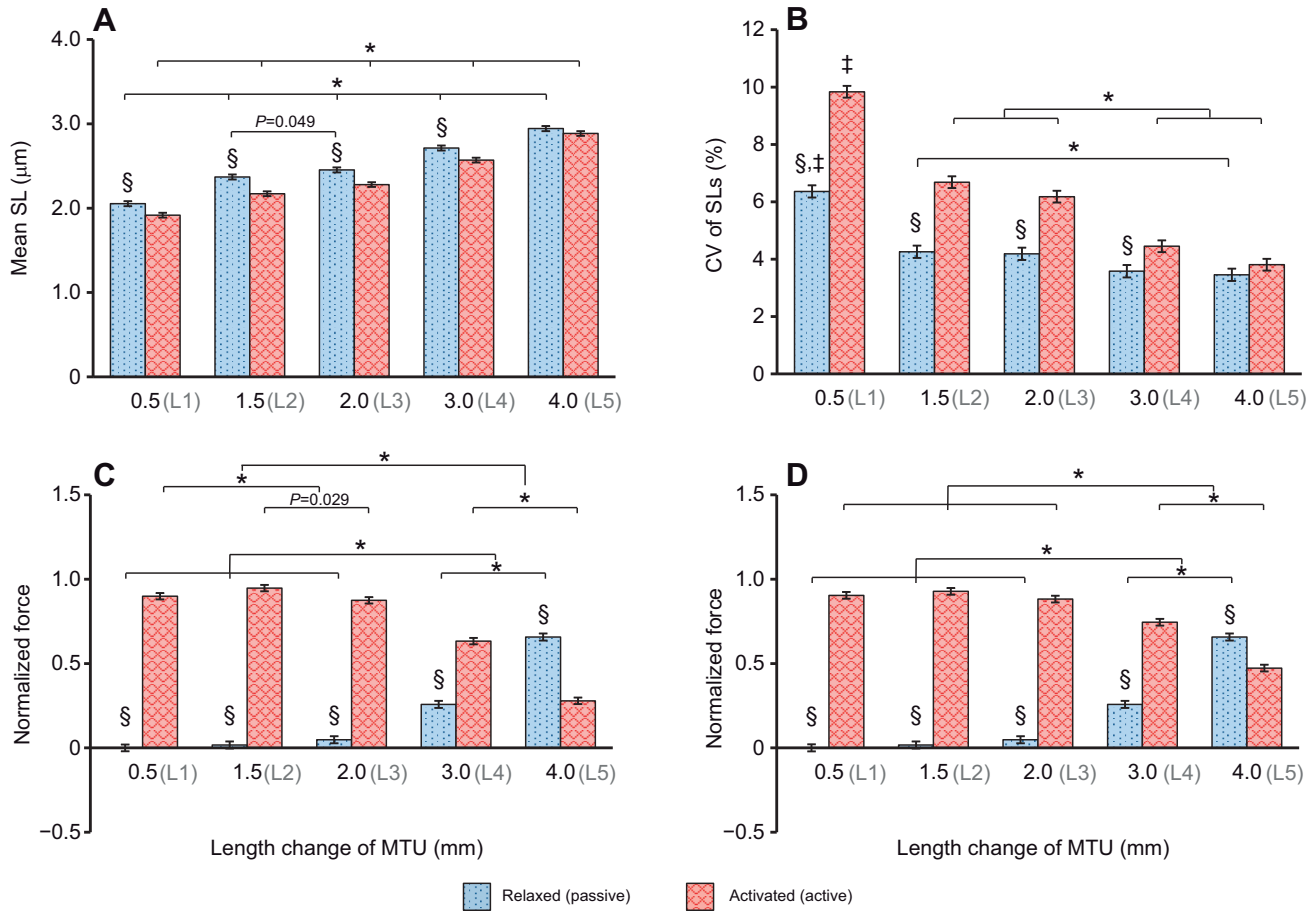

Fig. 3. Morphometric measures and muscle forces of mouse TAs (*n*=6) at five MTU lengths. (A,B) Morphometric measures were derived from individual image bands in the form of (A) mean SL and (B) coefficient of variation (CV) of SLs. (C,D) From the total force measured in maximally activated MTUs, active and passive forces were derived using (C) the standard and (D) the structural Hill model. The forces were normalized to the highest isometric force recorded in individual muscles. *Significant difference between different muscle length groups (P<0.01). §Significant difference when compared with the activated state at the corresponding muscle length (P<0.01). ‡Significant difference between L1 and the rest of the MTU length groups (P<0.01). P-values deviating from these values are indicated in the figure.

three-element rheological models introduced by Hill (Hill, 1938), which yielded standard and structural muscle forces, respectively (Fig. 1). The passive sarcomere FL data collected from six animals are plotted in Fig. 4, and were best fitted with an exponential curve that was used to determine the structural active forces (see Materials and Methods). Passive force was observed when the TA was stretched to lengths that corresponded to mean SLs of >2.4 μm (L2–5 conditions; Fig. 3C,D) (Wood et al., 2014). The active forces were higher than the passive forces when the muscles were stretched by 4–27% strain (L1–4 conditions). But when the muscles were stretched by 31–36% from their resting lengths (L5 condition), the passive forces became greater than the active forces (Fig. 3C,D), which, not surprisingly, coincided with no shortening of sarcomeres upon muscle activation (Fig. 3A).

The experimental FL curve exhibited the typical inverted U-shape (Figs 5 and 6). The FL curve constructed using the SLs measured in the relaxed muscles did not fit either of the two theoretical FL curves, and was shifted to the right of the theoretical curve on the ascending limb and plateau region, and had a steeper descending limb than the theoretical curve when assuming a thin filament length of 0.95 μm (Fig. 5A). When using SLs measured in the activated muscles, the experimental FL curve approximated closely the theoretical FL curve for an assumed thin filament length of 0.95 μm, as published by Gokhin et al. (2014, 2015) (black curve in Figs 5B,C and 6). The structural Hill model (Fig. 1A, right) was better than the standard Hill model in capturing the passive and active force contributions of the mouse TA (yellow band, Figs 5B,C and 6). The descending limb of the experimental FL curve constructed using the passive SL–standard Hill model, the active SL–standard Hill model and the active SL–structural Hill model (Fig. 5) had root mean square deviation of 0.14, 0.15 and 0.08 μm from the theoretical curve, respectively.

DISCUSSION

Here, we measured *in situ* individual SLs and muscle forces in maximally contracting isometric MTUs of TA, thereby eliminating assumptions implicitly made when estimating SL changes from muscle length changes. Contrary to our hypothesis, the average values of the SLs measured from less than one-millionth of all sarcomeres from the TA muscle predicted well the relative muscle forces obtained theoretically for a single sarcomere based on the sliding filament theory (Fig. 5C).

For proper predictions of the FL relationship of an entire muscle from the average SL, at least three factors need to be carefully considered. (i) Rather than using SLs measured from relaxed muscles (Fig. 5A), as has been done in studies where SL was derived from cadaveric specimens (Cutts, 1988; Lutz and Rome,

Journal of Experimental Biology (2020) 223, jeb215020. doi:10.1242/jeb.215020

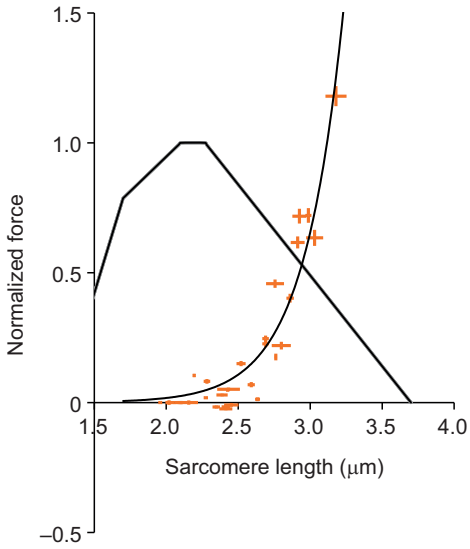

Fig. 4. Scatter plots of the passive sarcomere FL data. Each data point represents the mean (mid-point) ±s.d. (horizontal and vertical error bars) SL and muscle force measured in the relaxed muscles held at five MTU lengths. The black inverted U-shaped curve represents the theoretical FL curve constructed using thin filament lengths of 0.95 µm (Gokhin et al., 2014, 2015). An exponential curve was best fitted to the measured passive FL data.

1994; Mai and Lieber, 1990; Moo et al., 2017b; Rack and Westbury, 1969; Vaz et al., 2012), SLs need to be known for the active state of the muscle at each muscle length. This is not necessarily trivial as sarcomere shortening upon (fixed-end isometric) muscle activation depends crucially on the initial length of the muscle and its force capacity at that length (Fig. 3A), especially for MTUs with substantial free tendon length, like the mouse TA used in this study. For MTUs with a negligible free tendon length, the activation-induced shortening of sarcomeres may be small enough that it is sufficient to use the SLs from the relaxed muscles for the prediction of the FL relationship of a muscle. (ii) Actin and myosin filament lengths of the target muscle need to be known. Actin and myosin filament lengths can vary between species (Herzog et al., 1992a; Walker and Schrodt, 1974), within a given muscle (fast twitch versus slow twitch) (Gokhin et al., 2012; Granzier et al., 1991) and as a function of age (Gokhin et al., 2014). For the mouse TA, actin filament lengths in the literature vary from 0.95 to 1.20 µm (Gokhin et al., 2014, 2015; Pfeffer et al., 2011; Witt et al., 2006). These variations are associated with the age of the animals, and the assumptions that researchers have made about the definition of the functional length of the actin filaments. As only the free filamentous-actins (F-actins) within the sarcomere I-band interact with myosin cross-bridges, actin filament lengths should be defined by this functional region, and exclude the Z-line and the tropomodulin that caps the pointed-end of thin filaments. (iii) The passive forces in the intact MTU need to be properly accounted for. In terms of the Hill model, this means that estimates of passive forces originating from the visco-elastic components (Fig. 1A), such as the collagenous extracellular matrix at the tissue level (Gillies and Lieber, 2011; Purslow, 2008) and titin at the sarcomere level (Joumaa et al., 2008; Leonard and Herzog, 2010; Powers et al., 2017), need to be carefully done. As sarcomeres in the intact MTU shorten upon (fixed-end isometric) activation, proper subtraction of passive forces, which correspond to the instantaneous average SLs (structural force in Fig. 1B), becomes particularly important at long muscle lengths when passive forces change rapidly for small changes in muscle/sarcomere lengths.

It is worthwhile pointing out that although our results show that the mean SL measured in the mid-belly of the TA predicted the theoretical (sliding filament-based) FL relationship well, they are in contrast to many previous results of fixed-end contractions in single muscle fibres, which exhibit a vastly increased plateau area and much greater forces on the descending limb of the FL relationship (Granzier and Pollack, 1990; Iwazumi and Pollack, 1981; Pollack, 1990; Ramsey and Street, 1940; ter Keurs et al., 1978) than expected based on the theoretical sliding filament assumption (Gordon et al.,

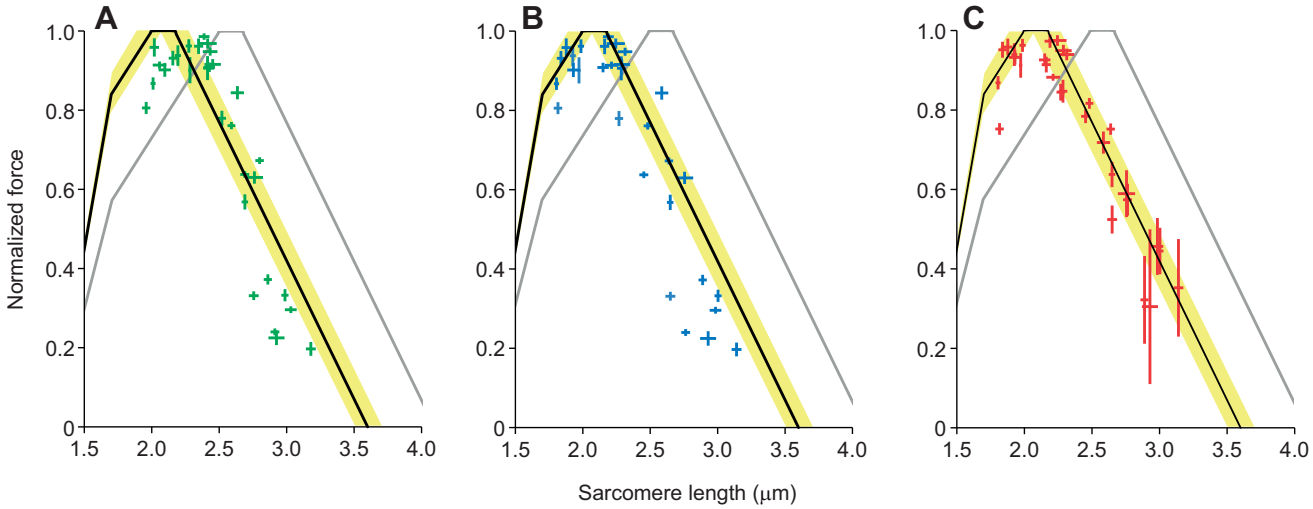

Fig. 5. Scatter plots of the sarcomere FL data using 'standard' and 'structural' active forces, and SLs measured in relaxed and activated muscles. (A) Standard active force versus SL in relaxed muscles. (B) Standard active force versus SL in activated muscles. (C) Structural active force versus SL in activated muscles. There are 30 data points in each graph representing the mean (mid-point) ±s.d. (horizontal and vertical error bars) of SLs and muscle forces measured in six muscles held at five MTU lengths. B and C were constructed using data presented in Fig. 6. The active and passive forces were normalized by the highest isometric active force recorded in the individual muscles. The black and grey inverted U-shaped curves represent the theoretical FL curve constructed using thin filament lengths of 0.95 µm (Gokhin et al., 2014, 2015) and 1.2 µm (Witt et al., 2006), respectively. The yellow shading around the black curve represents the standard deviation of thin filament lengths measured by Gokhin et al. (2015).

Journal of Experimental Biology (2020) 223, jeb215020. doi:10.1242/jeb.215020

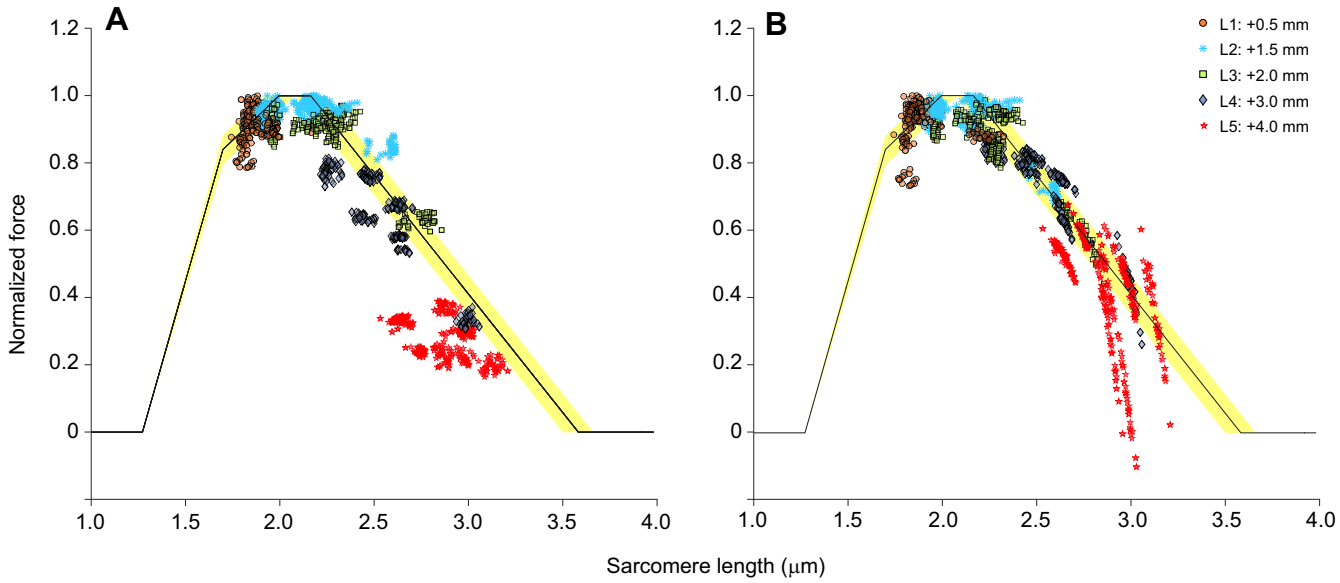

Fig. 6. Scatter plot of all sarcomere FL data using standard and structural active forces. (A) Standard active forces and (B) structural active forces versus SL for *n*=6 muscles. Each data point represents the average SL in individual image bands (as shown in Fig. 1B) and the corresponding active force at the same time (see Materials and Methods). The solid curve represents the theoretical FL curve built assuming a thin filament length of 0.95 µm (Gokhin et al., 2014, 2015). Forces were normalized relative to the highest isometric force recorded in each individual muscle. The yellow shading around the theoretical curve represents the standard deviation of thin filament lengths measured by Gokhin et al. (2015). Note that because of the exponential nature of the passive FL curve used for the derivation of the structural active force (Fig. 4), the slope of the curve at long SL was steep. Therefore, a small variation in SL leads to a great difference in the resulting structural passive force, thus leading to the large data spread at long SLs (B; L5).

1966). Similar to the deviations of fixed-end single-fibre FL relationships, we expected the fixed-end whole-muscle FL curve to show a broader plateau and greater forces on the descending limb of the FL relationship than that theoretically predicted by the sliding filament theory. Furthermore, our experiments on intact MTUs have completely different boundary conditions from the classic experiments performed by Gordon et al. (1966), where they experimentally derived the theoretical FL relationship for a single sarcomere, specifically with regards to the way they obtained force and SL. First, the force in their paper was not a measured force. Instead, they approximated the force rise upon activation and the creep force once the muscle was fully activated with two straight lines, and used the intersection of these two lines as the 'steady-state isometric' force. Furthermore, they preceded some of their isometric force measurements with an active shortening contraction, which we now know is associated with a decrease in the steady-state isometric force at the final target length as a result of the so-called residual force depression property of skeletal muscle (Joumaa and Herzog, 2010). Second, the sarcomere length in their paper was not directly measured, but was assumed constant in a mid-fibre segment whose length was kept constant by a feedback control system. However, in order to keep this mid-fibre segment at a constant length, one end of the fibre was continuously adjusted, thereby causing an overall length change of the fibre during these so-called isometric contractions. Despite the differences in experimental conditions, our results agree well with the theoretical sarcomere FL relationship (Gordon et al., 1966). The exact reason for such good agreement between the two results is currently unknown.

Also, the effect of SL non-uniformity on the FL properties of the whole muscle remains unclear. Our results suggest that SLs within a tiny volume of mid-TA were dispersed greatly with a CV of up to 10% (Fig. 3B). These large variations in SL have also been observed in single myofibrils where all sarcomeres are arranged mechanically in series, and therefore must carry the same amount of force. It remains unknown how myofilament overlap and intra-sarcomeric structural proteins (e.g. titin) interact to affect force production in neighbouring sarcomeres with vast SL non-uniformity, either in a single myofibril or in a fibre or a muscle, as tested here. Furthermore, the SL non-uniformity observed in a tiny region of the muscle is even greater when sarcomeres from other sites of the muscle are included, thereby further exaggerating the non-uniformity (Moo and Herzog, 2018; Moo et al., 2017a). It is currently unclear why SL non-uniformity exists across all structural levels of muscle, and how its presence affects the mechanical properties of muscles. Interestingly, indirect flight muscles of insects often have highly uniform sarcomeres. These muscles have a high intrinsic stiffness through passive structural proteins that provide an integrity (Bullard et al., 2006) that does not seem to be part of skeletal muscles in vertebrate animals. Because of the high stiffness, their excursion is small but it allows for fast wing beat action (Chan and Dickinson, 1996; Gilmour and Ellington, 1993; Josephson et al., 2000). Muscles with large excursions would be ill served with high passive stiffness, but the low passive stiffness may allow for the sarcomere length non-uniformities that are observed in most skeletal muscles, and these non-uniformities may be a negative side effect that muscles with low stiffness and vast excursions must tolerate to function properly.

There are limitations in the current study that need to be taken into account for proper interpretation of our results. First, similar to laser diffraction techniques that rely on the grating patterns of sarcomeres, SHG imaging can only be used confidently when SLs are longer than about 1.6 µm, as shorter SLs will render adjacent myosin bands indistinguishable. Second, the passive force development in relaxed and activated muscles is not well defined and probably differs between passive and active muscles (Labeit et al., 2003; Leonard and Herzog, 2010). It has been shown that the structural protein titin can change its stiffness upon muscle activation in a variety of ways; for example, by binding of calcium to specific sites on titin (DuVall

et al., 2013; Labeit et al., 2003). Recent studies also found that not all parts of titin can easily unfold in the active state (for reasons that are not fully understood yet) (DuVall et al., 2017), thus shortening the free spring length of titin and leading to an increase of titin's passive force contribution in the active compared with the passive muscle (Dutta et al., 2018; Powers et al., 2014). In the present study, we did not consider this aspect, as it seems impossible to account for the potential changes in passive force upon muscle activation while the molecular details of these events remain unknown. Therefore, current approaches of using passive sarcomere FL curves (Fig. 4) to obtain passive forces in active muscles may be inappropriate, and they probably underestimate the true passive force contributions in an active muscle. Finally, as SL distribution and changes in SL with changing muscle length are heterogeneous across whole muscles (Moo et al., 2016; O'Connor et al., 2016), our results are only applicable to SLs measured at the mid-belly of the mouse TA. It will be interesting to explore whether our results also hold for muscles other than the mouse TA tested here.

Conclusion

We conclude that the *in situ* mean SLs measured in the mid-belly of the maximally contracting mouse TA predict muscle force in accordance with the standard sliding filament model for single sarcomeres. Consistent with the literature, we found that the structural Hill model is a better model than the standard Hill model in deriving active muscle force from the total force measured in maximally activated MTUs. Also, SLs measured in the relaxed muscles led to a rightward shift of the sarcomere FL curve on the ascending limb and the plateau, and a steeper descending limb, and thus erroneous interpretation of the working range of sarcomeres in the intact MTU. Our findings may be applied in clinical settings, such as assessing functional deficits in patients with muscle diseases, by using a commercially available micro-endoscopy system that allows measurement of *in vivo* human SLs under twitch stimulation (Sanchez et al., 2015). Theoretical modelling of skeletal muscle properties will also benefit from our results through improvements to the characterization of input parameters into such models. Further studies should be conducted to test whether the sarcomere FL relationship, as determined here, also holds for other muscles, and for intact cardiac muscles.

Acknowledgements

The authors would like to thank Mr Andrew Sawatsky for help in animal surgery, Dr Ziad Abusara for maintaining the multi-photon microscope, Mr Andrzej Stano for maintaining the force transducer, Mr Scott Sibole, Dr Rafael Fortuna, Dr Venus Joumaa and Dr Ian Smith for useful discussion on data interpretation, and Dr Tak-Shing Fung for help with statistical analysis.

Competing interests

The authors declare no competing or financial interests.

Author contributions

Conceptualization: E.K.M., T.R.L., W.H.; Methodology: E.K.M., T.R.L., W.H.; Software: E.K.M.; Validation: E.K.M., T.R.L., W.H.; Formal analysis: E.K.M., T.R.L., W.H.; Investigation: E.K.M., T.R.L., W.H.; Resources: T.R.L., W.H.; Data curation: E.K.M., T.R.L., W.H.; Writing - original draft: E.K.M.; Writing - review & editing: E.K.M., T.R.L., W.H.; Visualization: E.K.M., T.R.L., W.H.; Supervision: T.R.L., W.H.; Project administration: E.K.M., T.R.L., W.H.; Funding acquisition: W.H.

Funding

This study was supported by an Alberta Innovates - Health Solutions postdoctoral fellowship (grant number: 10013510), a Canadian Institutes of Health Research postdoctoral fellowship (grant number: 10010953), the Killam Foundation, the Canada Research Chairs Programme, and the Natural Sciences and Engineering Research Council of Canada.

Data availability

Data are available from ResearchGate: https://www.researchgate.net/publication/339848678_Experimental_data_used_in_Moo_et_al_JEB_2020.

Supplementary information

Supplementary information available online at http://jeb.biologists.org/lookup/doi/10.1242/jeb.215020.supplemental

References

Arampatzis, A., Karamanidis, K., Stafilidis, S., Morey-Klapsing, G., DeMonte, G. and Brüggemann, G.-P. (2006). Effect of different ankle- and knee-joint positions on gastrocnemius medialis fascicle length and EMG activity during isometric plantar flexion. *J. Biomech.* **39**, 1891-1902. doi:10.1016/j.jbiomech.2005.05.010

Azizi, E., Brainerd, E. L. and Roberts, T. J. (2008). Variable gearing in pennate muscles. *Proc. Natl. Acad. Sci. USA* **105**, 1745-1750. doi:10.1073/pnas.0709212105

Blemker, S. S., Pinsky, P. M. and Delp, S. L. (2005). A 3D model of muscle reveals the causes of nonuniform strains in the biceps brachii. *J. Biomech.* **38**, 657-665. doi:10.1016/j.jbiomech.2004.04.009

Bullard, B., Garcia, T., Benes, V., Leake, M. C., Linke, W. A. and Oberhauser, A. F. (2006). The molecular elasticity of the insect flight muscle proteins projectin and kettin. *Proc. Natl. Acad. Sci. USA* **103**, 4451-4456. doi:10.1073/pnas.0509016103

Burkholder, T. J., Fingado, B., Baron, S. and Lieber, R. L. (1994). Relationship between muscle fiber types and sizes and muscle architectural properties in the mouse hindlimb. *J. Morphol.* **221**, 177-190. doi:10.1002/jmor.1052210207

Chan, W. P. and Dickinson, M. H. (1996). In vivo length oscillations of indirect flight muscles in the fruit fly Drosophila virilis. *J. Exp. Biol.* **199**, 2767-2774.

Cromie, M. J., Sanchez, G. N., Schnitzer, M. J. and Delp, S. L. (2013). Sarcomere lengths in human extensor carpi radialis brevis measured by microendoscopy. *Muscle Nerve* **48**, 286-292. doi:10.1002/mus.23760

Cutts, A. (1988). The range of sarcomere lengths in the muscles of the human lower limb. *J. Anat.* **160**, 79-88.

de Brito Fontana, H. and Herzog, W. (2016). Vastus lateralis maximum force-generating potential occurs at optimal fascicle length regardless of activation level. *Eur. J. Appl. Physiol.* **116**, 1267-1277. doi:10.1007/s00421-016-3381-3

Dumonceaux, J., Marie, S., Beley, C., Trollet, C., Vignaud, A., Ferry, A., Butler-Browne, G. and Garcia, L. (2010). Combination of myostatin pathway interference and dystrophin rescue enhances tetanic and specific force in dystrophic mdx mice. *Mol. Ther.* **18**, 881-887. doi:10.1038/mt.2009.322

Dutta, S., Tsiros, C., Sundar, S. L., Athar, H., Moore, J., Nelson, B., Gage, M. J. and Nishikawa, K. (2018). Calcium increases titin N2A binding to F-actin and regulated thin filaments. *Sci. Rep.* **8**, 14575. doi:10.1038/s41598-018-32952-8

DuVall, M. M., Gifford, J. L., Amrein, M. and Herzog, W. (2013). Altered mechanical properties of titin immunoglobulin domain 27 in the presence of calcium. *Eur. Biophys. J.* **42**, 301-307. doi:10.1007/s00249-012-0875-8

DuVall, M. M., Jinha, A., Schappacher-Tilp, G., Leonard, T. R. and Herzog, W. (2017). Differences in titin segmental elongation between passive and active stretch in skeletal muscle. *J. Exp. Biol.* **220**, 4418-4425. doi:10.1242/jeb.160762

Fukunaga, T., Ichinose, Y., Ito, M., Kawakami, Y. and Fukashiro, S. (1997). Determination of fascicle length and pennation in a contracting human muscle in vivo. *J. Appl. Physiol.* **82**, 354-358. doi:10.1152/jappl.1997.82.1.354

Gillies, A. R. and Lieber, R. L. (2011). Structure and function of the skeletal muscle extracellular matrix. *Muscle Nerve* **44**, 318-331. doi:10.1002/mus.22094

Gilmour, K. M. and Ellington, C. P. (1993). In vivo muscle length changes in bumblebees and the in vitro effects on work and power. *J. Exp. Biol.* **183**, 101-113.

Gokhin, D. S., Bang, M.-L., Zhang, J., Chen, J. and Lieber, R. L. (2009). Reduced thin filament length in nebulin-knockout skeletal muscle alters isometric contractile properties. *Am. J. Physiol. Cell Physiol.* **296**, C1123-C1132. doi:10.1152/ajpcell.00503.2008

Gokhin, D. S., Kim, N. E., Lewis, S. A., Hoenecke, H. R., D'Lima, D. D. and Fowler, V. M. (2012). Thin-filament length correlates with fiber type in human skeletal muscle. *Am. J. Physiol. Cell Physiol.* **302**, C555-C565. doi:10.1152/ajpcell.00299.2011

Gokhin, D. S., Dubuc, E. A., Lian, K. Q., Peters, L. L. and Fowler, V. M. (2014). Alterations in thin filament length during postnatal skeletal muscle development and aging in mice. *Front. Physiol.* **5**. doi:10.3389/fphys.2014.00375

Gokhin, D. S., Ochala, J., Domenighetti, A. A. and Fowler, V. M. (2015). Tropomodulin 1 directly controls thin filament length in both wild-type and tropomodulin 4-deficient skeletal muscle. *Development* **142**, 4351-4362. doi:10.1242/dev.129171

Gordon, A. M., Huxley, A. F. and Julian, F. J. (1966). The variation in isometric tension with sarcomere length in vertebrate muscle fibres. *J. Physiol.* **184**, 170-192. doi:10.1113/jphysiol.1966.sp007909

Granzier, H. L. and Pollack, G. H. (1990). The descending limb of the force-sarcomere length relation of the frog revisited. *J. Physiol.* **421**, 595-615. doi:10.1113/jphysiol.1990.sp017964

Granzier, H. L., Akster, H. A. and Ter Keurs, H. E. (1991). Effect of thin filament length on the force-sarcomere length relation of skeletal muscle. *Am. J. Physiol.* **260**, C1060-C1070. doi:10.1152/ajpcell.1991.260.5.C1060

Heemskerk, A. M., Strijkers, G. J., Vilanova, A., Drost, M. R. and Nicolay, K. (2005). Determination of mouse skeletal muscle architecture using three-dimensional diffusion tensor imaging. *Magn. Reson. Med.* **53**, 1333-1340. doi:10.1002/mrm.20476

Herzog, W., Kamal, S. and Clarke, H. D. (1992a). Myofilament lengths of cat skeletal muscle: theoretical considerations and functional implications. *J. Biomech.* **25**, 945-948. doi:10.1016/0021-9290(92)90235-S

Herzog, W., Leonard, T. R., Renaud, J. M., Wallace, J., Chaki, G. and Bornemisza, S. (1992b). Force-length properties and functional demands of cat gastrocnemius, soleus and plantaris muscles. *J. Biomech.* **25**, 1329-1335. doi:10.1016/0021-9290(92)90288-C

Hill, A. V. (1938). The heat of shortening and the dynamic constants of muscle. *Proc. R. Soc. Lond. B Biol. Sci.* **126**, 136-195. doi:10.1098/rspb.1938.0050

Holt, N. C., Danos, N., Roberts, T. J. and Azizi, E. (2016). Stuck in gear: age-related loss of variable gearing in skeletal muscle. *J. Exp. Biol.* **219**, 998-1003. doi:10.1242/jeb.133009

Huxley, A. F. and Peachey, L. D. (1961). The maximum length for contraction in vertebrate striated muscle. *J. Physiol.* **156**, 150-165. doi:10.1113/jphysiol.1961.sp006665

Infantolino, B. W., Ellis, M. J. and Challis, J. H. (2010). Individual sarcomere lengths in whole muscle fibers and optimal fiber length computation. *Anat. Rec. Adv. Integr. Anat. Evol. Biol.* **293**, 1913-1919. doi:10.1002/ar.21239

Iwazumi, T. and Pollack, G. H. (1981). The effect of sarcomere non-uniformity on the sarcomere length-tension relationship of skinned fibers. *J. Cell. Physiol.* **106**, 321-337. doi:10.1002/jcp.1041060302

Johnston, K., Jinha, A. and Herzog, W. (2016). The role of sarcomere length non-uniformities in residual force enhancement of skeletal muscle myofibrils. *R. Soc. Open Sci.* **3**, 150657. doi:10.1098/rsos.150657

Johnston, K., Moo, E. K., Jinha, A. and Herzog, W. (2019). On sarcomere length stability during isometric contractions before and after active stretching. *J. Exp. Biol.* **222**, jeb209924. doi:10.1242/jeb.209924

Josephson, R. K., Malamud, J. G. and Stokes, D. R. (2000). Asynchronous muscle: a primer. *J. Exp. Biol.* **203**, 2713-2722.

Joumaa, V. and Herzog, W. (2010). Force depression in single myofibrils. *J. Appl. Physiol.* **108**, 356-362. doi:10.1152/japplphysiol.01108.2009

Joumaa, V., Leonard, T. R. and Herzog, W. (2008). Residual force enhancement in myofibrils and sarcomeres. *Proc. R. Soc. B* **275**, 1411-1419. doi:10.1098/rspb.2008.0142

Julian, F. J. and Morgan, D. L. (1979). The effect on tension of non-uniform distribution of length changes applied to frog muscle fibres. *J. Physiol.* **293**, 379-392. doi:10.1113/jphysiol.1979.sp012895

Labeit, D., Watanabe, K., Witt, C., Fujita, H., Wu, Y., Lahmers, S., Funck, T., Labeit, S. and Granzier, H. (2003). Calcium-dependent molecular spring elements in the giant protein titin. *Proc. Natl. Acad. Sci. USA* **100**, 13716-13721. doi:10.1073/pnas.2235652100

Leonard, T. R. and Herzog, W. (2010). Regulation of muscle force in the absence of actin-myosin-based cross-bridge interaction. *Am. J. Physiol. Cell Physiol.* **299**, C14-C20. doi:10.1152/ajpcell.00049.2010

Lichtwark, G. A., Farris, D. J., Chen, X., Hodges, P. W. and Delp, S. L. (2018). Microendoscopy reveals positive correlation in multiscale length changes and variable sarcomere lengths across different regions of human muscle. *J. Appl. Physiol.* **125**, 1812-1820. doi:10.1152/japplphysiol.00480.2018

Llewellyn, M. E., Barretto, R. P. J., Delp, S. L. and Schnitzer, M. J. (2008). Minimally invasive high-speed imaging of sarcomere contractile dynamics in mice and humans. *Nature* **454**, 784-788. doi:10.1038/nature07104

Lovering, R. M., Shah, S. B., Pratt, S. J. P., Gong, W. and Chen, Y. (2013). Architecture of healthy and dystrophic muscles detected by optical coherence tomography. *Muscle Nerve* **47**, 588-590. doi:10.1002/mus.23711

Lutz, G. J. and Rome, L. C. (1994). Built for jumping: the design of the frog muscular system. *Science* **263**, 370-372. doi:10.1126/science.8278808

Maas, H., Baan, G. C. and Huijing, P. A. (2001). Intermuscular interaction via myofascial force transmission: effects of tibialis anterior and extensor hallucis longus length on force transmission from rat extensor digitorum longus muscle. *J. Biomech.* **34**, 927-940. doi:10.1016/S0021-9290(01)00055-0

MacIntosh, B. R. and MacNaughton, M. B. (2005). The length dependence of muscle active force: considerations for parallel elastic properties. *J. Appl. Physiol.* **98**, 1666-1673. doi:10.1152/japplphysiol.01045.2004

Mai, M. T. and Lieber, R. L. (1990). A model of semitendinosus muscle sarcomere length, knee and hip joint interaction in the frog hindlimb. *J. Biomech.* **23**, 271-279. doi:10.1016/0021-9290(90)90017-W

Moo, E. K. and Herzog, W. (2018). Single sarcomere contraction dynamics in a whole muscle. *Sci. Rep.* **8**, 15235. doi:10.1038/s41598-018-33658-7

Moo, E. K., Fortuna, R., Sibole, S. C., Abusara, Z. and Herzog, W. (2016). In vivo sarcomere lengths and sarcomere elongations are not uniform across an intact muscle. *Front. Physiol.* **187**. doi:10.3389/fphys.2016.00187

Moo, E. K., Leonard, T. R. and Herzog, W. (2017a). In vivo sarcomere lengths become more non-uniform upon activation in intact whole muscle. *Front. Physiol.* **8**. doi:10.3389/fphys.2017.01015

Moo, E. K., Peterson, D. R., Leonard, T. R., Kaya, M. and Herzog, W. (2017b). In vivo muscle force and muscle power during near-maximal frog jumps. *PLoS ONE* **12**, e0173415. doi:10.1371/journal.pone.0173415

O'Connor, S. M., Cheng, E. J., Young, K. W., Ward, S. R. and Lieber, R. L. (2016). Quantification of sarcomere length distribution in whole muscle frozen sections. *J. Exp. Biol.* **219**, 1432-1436. doi:10.1242/jeb.132084

Pavlov, I., Novinger, R. and Rassier, D. E. (2009). Sarcomere dynamics in skeletal muscle myofibrils during isometric contractions. *J. Biomech.* **42**, 2808-2812. doi:10.1016/j.jbiomech.2009.08.011

Pfeffer, C. P., Olsen, B. R., Ganikhanov, F. and Légaré, F. (2011). Imaging skeletal muscle using second harmonic generation and coherent anti-Stokes Raman scattering microscopy. *Biomed. Opt. Express* **2**, 1366-1376. doi:10.1364/BOE.2.001366

Pollack, G. H. (ed.) (1990). The sliding-filament - cross-bridge theory: a critical evaluation. In *Muscles & Molecules: Uncovering the Principles of Biological Motion*, pp. 9-38. Ebner & Sons Publishers.

Powers, K., Schappacher-Tilp, G., Jinha, A., Leonard, T., Nishikawa, K. and Herzog, W. (2014). Titin force is enhanced in actively stretched skeletal muscle. *J. Exp. Biol.* **217**, 3629-3636. doi:10.1242/jeb.105361

Powers, K., Nishikawa, K., Joumaa, V. and Herzog, W. (2016). Decreased force enhancement in skeletal muscle sarcomeres with a deletion in titin. *J. Exp. Biol.* **219**, 1311-1316. doi:10.1242/jeb.132027

Powers, K., Joumaa, V., Jinha, A., Moo, E. K., Smith, I. C., Nishikawa, K. and Herzog, W. (2017). Titin force enhancement following active stretch of skinned skeletal muscle fibres. *J. Exp. Biol.* **220**, 3110-3118. doi:10.1242/jeb.153502

Purslow, P. P. (2008). The extracellular matrix of skeletal and cardiac muscle. In *Collagen* (ed. P. Fratzl), pp. 325-357. Springer US.

Rack, P. M. H. and Westbury, D. R. (1969). The effects of length and stimulus rate on tension in the isometric cat soleus muscle. *J. Physiol.* **204**, 443-460. doi:10.1113/jphysiol.1969.sp008923

Raiteri, B. J., Cresswell, A. G. and Lichtwark, G. A. (2018). Muscle-tendon length and force affect human tibialis anterior central aponeurosis stiffness in vivo. *Proc. Natl. Acad. Sci. USA* **115**, E3097-E3105. doi:10.1073/pnas.1712697115

Ramsey, R. W. and Street, S. F. (1940). The isometric length-tension diagram of isolated skeletal muscle fibers of the frog. *J. Cell. Comp. Physiol.* **15**, 11-34. doi:10.1002/jcp.1030150103

Rode, C., Siebert, T., Herzog, W. and Blickhan, R. (2009). The effects of parallel and series elastic components on the active cat soleus force-length relationship. *J. Mech. Med. Biol.* **09**, 105-122. doi:10.1142/S0219519409002870

Sanchez, G. N., Sinha, S., Liske, H., Chen, X., Nguyen, V., Delp, S. L. and Schnitzer, M. J. (2015). In vivo imaging of human sarcomere twitch dynamics in individual motor units. *Neuron* **88**, 1109-1120. doi:10.1016/j.neuron.2015.11.022

Sandercock, T. G. and Heckman, C. J. (2001). Whole muscle length-tension properties vary with recruitment and rate modulation in areflexive cat soleus. *J. Neurophysiol.* **85**, 1033-1038. doi:10.1152/jn.2001.85.3.1033

Telley, I. A., Denoth, J., Stüssi, E., Pfitzer, G. and Stehle, R. (2006). Half-sarcomere dynamics in myofibrils during activation and relaxation studied by tracking fluorescent markers. *Biophys. J.* **90**, 514-530. doi:10.1529/biophysj.105.070334

ter Keurs, H. E., Iwazumi, T. and Pollack, G. H. (1978). The sarcomere length-tension relation in skeletal muscle. *J. Gen. Physiol.* **72**, 565-592. doi:10.1085/jgp.72.4.565

Vaz, M. A., de la Rocha Freitas, C., Leonard, T. and Herzog, W. (2012). The force-length relationship of the cat soleus muscle. *Muscles Ligaments Tendons J.* **2**, 79-84.

Walker, S. M. and Schrodt, G. R. (1974). I segment lengths and thin filament periods in skeletal muscle fibers of the rhesus monkey and the human. *Anat. Rec.* **178**, 63-81. doi:10.1002/ar.1091780107

Willems, M. E. and Huijing, P. A. (1994). Heterogeneity of mean sarcomere length in different fibres: effects on length range of active force production in rat muscle. *Eur. J. Appl. Physiol.* **68**, 489-496. doi:10.1007/BF00599518

Winters, J. M. (1990). Hill-based muscle models: a systems engineering perspective. In *Multiple Muscle Systems: Biomechanics and Movement Organization* (ed. J. M. Winters and S. L.-Y. Woo), pp. 69-93. New York, NY: Springer New York.

Winters, T. M., Takahashi, M., Lieber, R. L. and Ward, S. R. (2011). Whole muscle length-tension relationships are accurately modeled as scaled sarcomeres in rabbit hindlimb muscles. *J. Biomech.* **44**, 109-115. doi:10.1016/j.jbiomech.2010.08.033

Witt, C. C., Burkart, C., Labeit, D., McNabb, M., Wu, Y., Granzier, H. and Labeit, S. (2006). Nebulin regulates thin filament length, contractility, and Z-disk structure in vivo. *EMBO J.* **25**, 3843-3855. doi:10.1038/sj.emboj.7601242

Wood, L. K., Kayupov, E., Gumucio, J. P., Mendias, C. L., Claflin, D. R. and Brooks, S. V. (2014). Intrinsic stiffness of extracellular matrix increases with age in skeletal muscles of mice. *J. Appl. Physiol.* **117**, 363-369. doi:10.1152/japplphysiol.00256.2014

Zhang, J., Zhang, G., Morrison, B., Mori, S. and Sheikh, K. A. (2008). Magnetic resonance imaging of mouse skeletal muscle to measure denervation atrophy. *Exp. Neurol.* **212**, 448-457. doi:10.1016/j.expneurol.2008.04.033

Table S1: Average and standard deviation of sarcomere lengths (SLs) measured from similar region of fixed fascicles by widefield light and multiphoton laser microscopies, respectively. The image analysis was the same as described in the Methods of the main text.

Fascicle	Total number of sarcomeres, Sn	Widefield light microscopy		Multiphoton laser microscopy	
		mean SL	SD	mean SL	SD
1	30	2.03	0.07	2.02	0.07
2	22	2.09	0.11	2.07	0.09
3	30	2.35	0.11	2.32	0.05
4	29	2.41	0.08	2.36	0.07
5	30	2.21	0.11	2.15	0.07

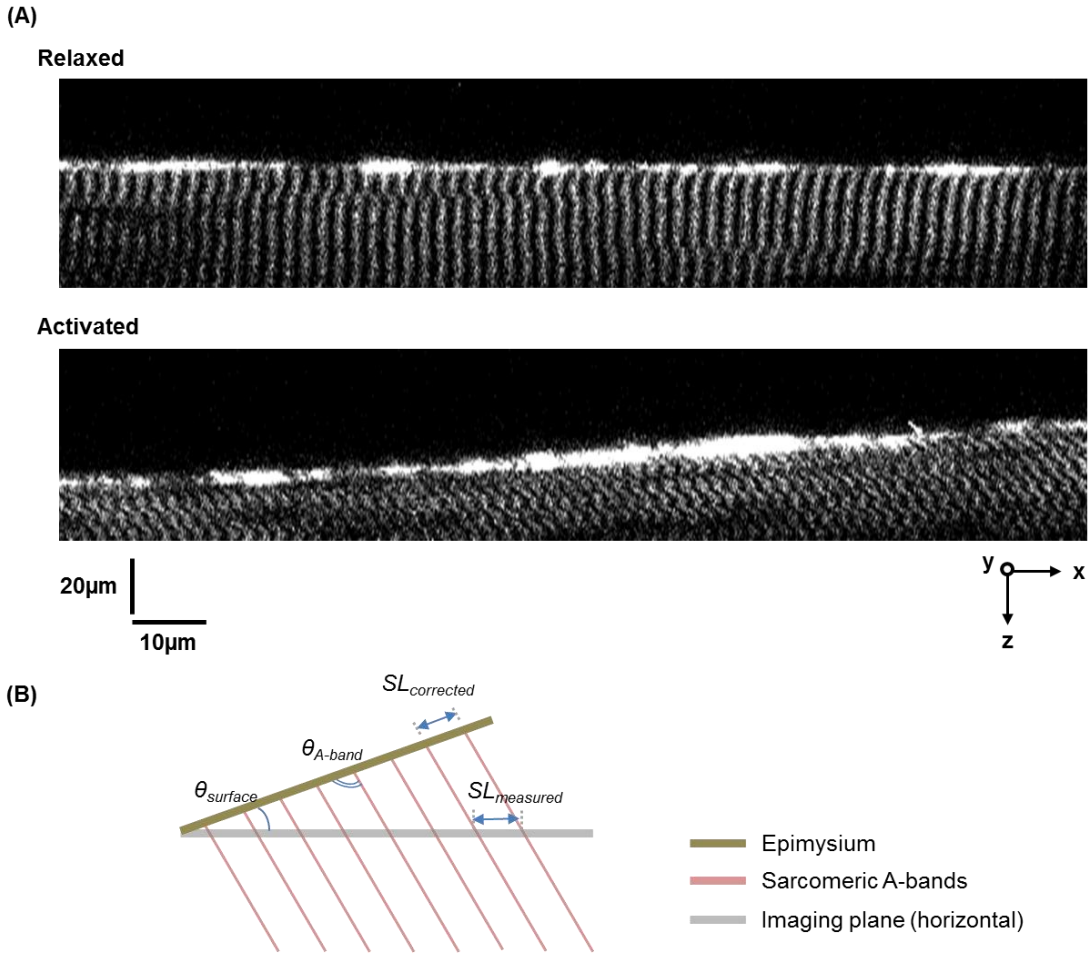

Fig. S1. Correction for out-of-plane orientation in sarcomere length (SL) measurements (A) Through-thickness muscle taken in the XZ-plane showing the orientations of the epimysium (top layer) and the sarcomeric A-bands (white bands) in the relaxed and activated muscle. (B) Schematic diagram showing the angles ($\theta_{surface}$ and $\theta_{A\text{-}band}$) measured from the through-thickness images in order to correct for the out-of-plane projection and obtain sarcomere lengths along the epimysium ($SL_{corrected}$).

Using the through-thickness muscle image in the XZ-plane (A), the orientation of the epimysium ($\theta_{surface}$) and the angle between the epimysium and the sarcomeric A-bands ($\theta_{A\text{-}band}$) were determined (B). As the time-series planar images of sarcomeres were taken in the horizontal plane, the SL measured ($SL_{measured}$) from this images were corrected for out-of-plane projection using the sine rule as shown in Eqn 1 and Eqn 2 to obtain SL along the epimysium ($SL_{corrected}$):

$$\frac{SL_{corrected}}{\sin(180-\theta_{surface}-\theta_{A-band})} = \frac{SL_{measured}}{\sin(\theta_{A-band})} \quad (1)$$

$$SL_{corrected} = \frac{\sin(180-\theta_{surface}-\theta_{A-band})}{\sin(\theta_{A-band})} \times SL_{measured} \quad (2)$$